Real-Time Adaptive Control for Haptic Telemanipulation With Kalman Active Observers

Rui Cortesão, *Member, IEEE*, Jaeheung Park, *Student Member, IEEE*, and Oussama Khatib, *Fellow, IEEE*

***Abstract*—This paper discusses robotic telemanipulation with Kalman active observers and online stiffness estimation. Operational space techniques, feedback linearization, discrete state space methods, augmented states, and stochastic design are used to control a robotic manipulator with a haptic device. Stiffness estimation only based on force data (measured, desired, and estimated forces) is proposed, avoiding explicit position information. Stability and robustness to stiffness errors are discussed, as well as real-time adaptation techniques. Telepresence is analyzed. Experiments show high performance in contact with soft and hard surfaces.**

***Index Terms*—Compliant motion control, haptics, Kalman active observers (AOBs), robotic manipulation, stiffness estimation, telepresence.**

I. Introduction

TOUCH sensations are essential for many telemanipulation tasks. Haptic devices integrated in robotic systems can provide the right framework to execute contact tasks with high performance. Such systems can be applied not only for industrial purposes [32], but also in the field of service robotics [14]. Typical applications include remote handling in dangerous environments [21], telesurgery [35], and interaction with virtual objects [18]. Telepresence is reached if the haptic feeling represents well the real contact. Augmented reality through high-fidelity force feedback can result in the emergence of new manipulation techniques, extending human dexterity.

Physical limits (e.g., time delay, bandwidth, and sampling time) and robustness requirements of the robotic setup have to be mapped into an optimal haptic feeling, which is coded into the control architecture. To design a controller, approximate and linearized models are frequently considered, allowing the extensive and rich theory of linear systems to be applied. A simple and modular control synthesis can be achieved by decentralized control, decoupling the overall system into several subsystems, in which autonomous local controllers are designed. Compliant motion tasks require special attention [34], since the task constraints change abruptly and the model parameters may have wide variations, particularly for very stiff and unstructured environments.

The literature on robotic teleoperation is very extensive. Several control techniques have been presented to cope with uncertainty, time delay, master/slave models, robustness, and telepresence. Zhu and Salcudean [38] proposed adaptive motion/force control robust to time delays, taking into account nonlinear rigid body dynamics of master/slave systems. Ryu and Kwon [33] proposed adaptive bilateral control without estimating environment parameters. Kim *et al.* [24] suggested local force feedback (shared compliant control) to provide a compliant slave robot for stiff contact. Adaptive techniques based on passive systems have been discussed by Hannaford and Ryu [19]. Simple architectures such as position–force[1] and position–position[2] have limited performance [13], [26]. Various implementations have used additional information (such as forces and accelerations) to achieve better telepresence [26], [28], [37]. Hashtrudi-Zaad and Salcudean [20] have shown that perfect telepresence can be obtained under ideal conditions using local force feedback with a three-channel architecture. Stability analysis has been done by Colgate and Hogan [5] using the passivity theory, and by Flemmer *et al.* [17] based on closed-loop transfer functions. Lawrence [26] analyzed the tradeoff between stability and telepresence, proposing a unified four-channel control architecture based on force and position signals. Kalman active observers (AOBs), introduced in [6] and [39], have been applied in several applications, such as force control of robotic manipulators [8], [9], [30], haptic manipulation [11], [12], [29], humanoids [31], and mobile systems [2], [4], [7], [27].

This paper describes a control architecture for haptic telemanipulation with AOBs and online stiffness estimation. The background motivation of this study is robotic-assisted surgery, where the surgeon and robot work in the same room. Therefore, the system time delay is small and the contact parameters can be lumped into a Cartesian stiffness. The teleoperation scheme keeps a position–position architecture, in which force commands are generated through virtual coupling. The main differences of our approach with respect to previous work are given here.

1) The slave side has a decentralized[3] adaptive compliant motion controller with Kalman AOBs. The AOB reformulates the Kalman filter to accomplish model-reference adaptive

Manuscript received October 13, 2005. This paper was recommended for publication by Associate Editor E. Papadopoulos and Editor K. Lynch upon evaluation of the reviewers' comments. This paper is an expanded version of papers published in the Proceedings of the International Conference on Intelligent Robots and Systems, 2003, pp. 2938–2943; the Proceedings of the International Conference on Intelligent Robots and Systems, 2005, pp. 3146–3151; and the Proceedings of the International Conference on Advanced Robotics, 2003, pp. 513–519.

R. Cortesão is with the Institute of Systems and Robotics, University of Coimbra, 3030 Coimbra, Portugal (e-mail: cortesao@isr.uc.pt).

J. Park and O. Khatib are with the Robotics Group, Stanford University, Stanford, CA 94305-9010 USA (e-mail: park73@robotics.stanford.edu; ok@robotics.stanford.edu).

Digital Object Identifier 10.1109/TRO.2006.878787

[1]Position commands on the master side and force commands on the slave side.

[2]Only position commands.

[3]In this paper, decentralized control means an independent control for each Cartesian dimension.

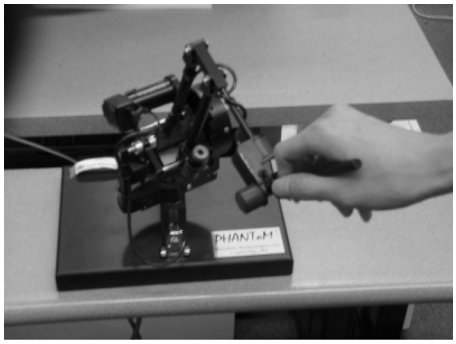

(a)

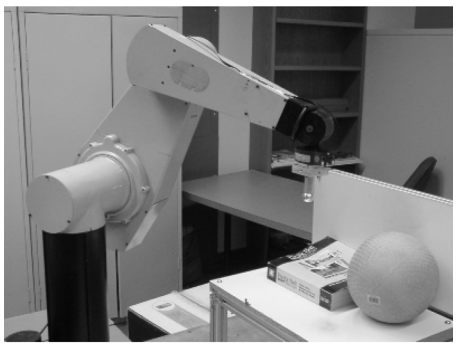

(b)

Fig. 1. System setup. (a) Phantom device controlled by a human. (b) PUMA robot. Soft and stiff objects belong to the PUMA workspace.

control, based on a desired closed-loop model, state augmentation, and stochastic design. The system stiffness enters in the AOB design, enabling consistent force responses (i.e., the same closed-loop dynamics) independent of contact objects.

2) Online stiffness estimation only based on force data (measured, desired, and estimated forces), avoiding explicit position information.

This paper is organized as follows. After the description of the system setup in Section II, the decentralized control architecture is presented in Section III. The AOB design is introduced in Section IV, including the AOB algorithm, estimation strategies, and control design. Stability and robustness to stiffness mismatches are discussed in Section V, including preliminary experiments on the slave side. Section VI describes the teleoperation scheme, analyzing telepresence and stability in free space and contact. The algorithm for online stiffness estimation is presented in Section VII. Haptic manipulation experiments are addressed in Section VIII. The conclusions are summarized in Section IX.

II. System Setup

Fig. 1 shows the master and slave stations. The master station is a Phantom 1.0A which has six degrees of freedom (DOFs) and three motors for the first joints. The haptic device is controlled by a quadric-processor Pentium Pro at 200 MHz. The slave robot is a PUMA 560, which has a stiff JR3 force sensor at the end-effector. The PUMA has six DOFs and is connected to a computer (Pentium II at 333 MHz with QNX real-time OS) through a TRC205 controller and a ServoToGo board. The control of the orientation is not considered in this setup. The PUMA robot is controlled so that it has the same orientation in a global frame. A local area network is used to connect both stations. The sampling time is $h = 2$ ms. The system time delay T_d was obtained experimentally. It is

$$T_d = 3h = 6 \text{ ms}. \tag{1}$$

The working space has objects with different stiffnesses. When the robot is manipulating, the system stiffness K_s is a function of the environment, the JR3 sensor, and the PUMA robot. If the environment is soft, K_s is approximately given by the environment stiffness. For stiff environments, the computation of K_s is not trivial.

TABLE I
Object Stiffnesses. K_s and $K_{s,n}$ Data

	free space	sponge	book	desk
K_s [N/m]	very small	300	stiff	stiff
$K_{s,n}$ [N/m]	100	Estimated	Estimated	Estimated

Table I presents experimental (K_s) and nominal $(K_{s,n})$ values of the system stiffness.[4] The relation between K_s and $K_{s,n}$ is

$$K_s = K_{s,n} + \Delta K_s \tag{2}$$

where ΔK_s is the error associated with $K_{s,n}$.

III. Decentralized Control Architecture

Here, we describe the decentralized control architecture applied in our system, based on operational space, feedback linearization, and state-space techniques.

A. Manipulator Dynamics

Given a set of generalized coordinates q (usually, joint angles for revolute joints) describing the robot's pose, the well-known robot dynamics is given by

$$M\ddot{q} + v(q, \dot{q}) + g(q) = \tau \tag{3}$$

where M is the mass matrix, $v(q, \dot{q})$ is the vector of Coriolis and centripetal forces, $g(q)$ is the gravity term, and τ is the generalized torque acting on q. For a nonredundant manipulator, (3) can be represented in the Cartesian domain by

$$\Lambda\ddot{X} + V_x(q, \dot{q}) + g_x(q) = F \tag{4}$$

with

$$\Lambda = J^{-T} M J^{-1} \tag{5}$$

$$V_x = J^{-T} v(q, \dot{q}) - \Lambda \dot{J}\dot{q} \tag{6}$$

$$\tau = J^T F \tag{7}$$

$$g_x = J^{-T} g(q) \tag{8}$$

where J, X, and F are, respectively, the Jacobian matrix, Cartesian position (operational space), and Cartesian force F [23]. An

[4]The nominal values are the ones used in the control design. The results of K_s for the sponge were achieved offline.

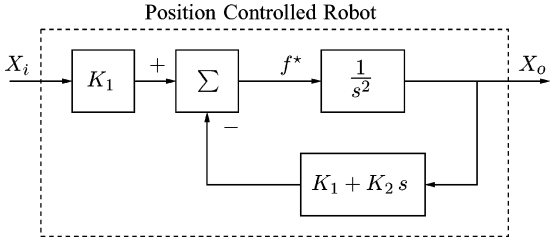

Fig. 2. Modification of the desired plant through feedback. X_i represents a position command, and X_o is the position output.

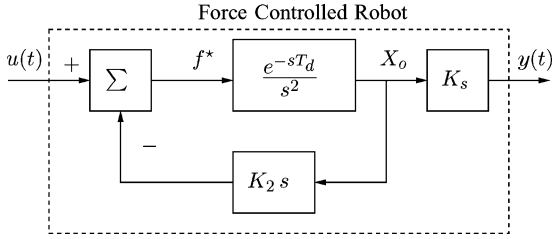

Fig. 3. System plant $G(s)$ for each Cartesian dimension. $u(t)$ is the force input, and $y(t)$ is the force output.

external force F_e always appears at the end-effector whenever the robot is in contact. Hence, (4) can be written as

$$\Lambda\ddot{X} + V_x(q,\dot{q}) + g_x(q) = F_c - F_e \tag{9}$$

where F_c is the force due to the commanded torque.

B. System Plant

If the desired system plant is

$$\ddot{X} = f^\star \tag{10}$$

then F_c should be[5]

$$F_c = \hat{F}_e + \hat{V}_x(q,\dot{q}) + \hat{g}_x(q) + \hat{\Lambda} f^\star. \tag{11}$$

Equation (10) defines a decoupled system for each Cartesian dimension with unitary mass. The estimation of F_e, $\hat{F}_e$ affects the control strategy, as will be explained in Section IV-B. The terms $\hat{V}_x(q,\dot{q})$, $\hat{g}_x(q)$, and $\hat{\Lambda}$ can be computed for a given robot. The estimation errors present in (11) corrupt (10). To increase robustness to model errors, the desired plant poles at the origin are "shifted" to the left using feedback, as shown in Fig. 2. For a critically damped response (damping factor $\zeta = 1$) with time constant τ_o, the feedback is given by

$$K_2 = \frac{2}{\tau_o} \quad \text{and} \quad K_1 = \frac{K_2^2}{4}. \tag{12}$$

The problem with this approach is that the force-controlled robot becomes a position-controlled robot (i.e., X_i is a position). External forces (e.g., human contact) applied to the robot's body experience a stiff contact due to position feedback. Eliminating the position loop and inserting T_d and K_s (see Fig. 3), the system plant becomes

$$G(s) = \frac{K_s e^{-sT_d}}{s(s + K_2 e^{-sT_d})}. \tag{13}$$

1) Small Time Delay: If T_d is small, (13) can be approximated by

$$G(s) \approx \frac{K_s e^{-sT_d}}{s(s + K_2)} \tag{14}$$

[5]The symbol ˆ means estimate.

for a wide range of frequencies. Its equivalent temporal representation is

$$\ddot{y}(t) + K_2\dot{y}(t) = K_s u(t - T_d) \tag{15}$$

where $y(t)$ is the plant output (Cartesian force at the robot's end-effector) and u is the plant input (force). Defining the state variables $x_1(t) = y(t)$ and $x_2(t) = \dot{y}(t)$, (15) can be written as

$$\begin{bmatrix}\dot{x}_1(t)\\ \dot{x}_2(t)\end{bmatrix} = \begin{bmatrix}0 & 1\\ 0 & -K_2\end{bmatrix}\begin{bmatrix}x_1(t)\\ x_2(t)\end{bmatrix} + \begin{bmatrix}0\\ K_s\end{bmatrix} u(t - T_\mathrm{d}). \tag{16}$$

In compact form, we have

$$\begin{cases}\dot{x}(t) = Ax(t) + Bu(t - T_d)\\ y(t) = x_1(t).\end{cases} \tag{17}$$

Discretizing (17) with sampling time h [1], the equivalent discrete-time system is

$$\begin{cases}x_{r,k} = \Phi_r x_{r,k-1} + \Gamma_r u_{k-1}\\ y_k = C_r x_{r,k}\end{cases} \tag{18}$$

with

$$T_d = (d-1)h + \tau' \tag{19}$$

$$0 < \tau' \le h \tag{20}$$

$$x_{r,k} = [x_k \quad u_{k-d} \quad \cdots \quad u_{k-2} \quad u_{k-1}]^T \tag{21}$$

$$\Phi_r = \begin{bmatrix}\Phi_1 & \Gamma_1 & \Gamma_0 & \cdots & 0\\ 0 & 0 & 1 & \cdots & 0\\ \vdots & \vdots & \vdots & \ddots & \vdots\\ 0 & 0 & 0 & \cdots & 1\\ 0 & 0 & 0 & \cdots & 0\end{bmatrix} \tag{22}$$

$$\Gamma_r = [0 \quad 0 \quad \cdots \quad 0 \quad 1]^T \tag{23}$$

$$C_r = [1 \quad 0 \quad \cdots \quad 0 \quad 0] \tag{24}$$

where Φ_1, Γ_0, and Γ_1 are given by

$$\Phi_1 = e^{Ah} = \phi(h) \tag{25}$$

$$\Gamma_0 = \int_0^{h-\tau'} \phi(\lambda)d\lambda B \tag{26}$$

$$\Gamma_1 = \phi(h - \tau') \int_0^{\tau'} \phi(\lambda)d\lambda B. \tag{27}$$

x_k has two states representing the force and force derivative. The other states appear due to T_d. The continuous state transition and command matrices are

$$\phi(t) = \begin{bmatrix} 1 & \frac{1-e^{-K_2 t}}{K_2} \\ 0 & e^{-K_2 t} \end{bmatrix} \quad \text{and} \quad B = \begin{bmatrix} 0 \\ K_s \end{bmatrix}. \tag{28}$$

From (28), the computation of Φ_1, Γ_0, and Γ_1 is straightforward.

2) Bigger Time Delays: If T_d is not small enough, the term

$$K_2 e^{-sT_d} \tag{29}$$

of (13) can be approximated by an adequate truncated Taylor series, increasing the system order. The same procedure of the small time delay can then be applied (not addressed in this paper).

IV. AOB Design

When some parameters of a controlled process have wide variations and are poorly known, high-performance controllers require adaptive control techniques. Landau [25] has defined adaptive systems as systems in which the adaptation mechanism modifies the parameters of the adjustable system or generates an auxiliary input to maintain a given index of performance bounded to acceptable values. To accomplish model-reference adaptive control, the AOB reformulates the Kalman filter, based on the following.

1) A desired closed-loop system (reference model) that enters in the state estimation.
2) An extra equation (auxiliary input) to estimate an equivalent disturbance referred to the system input, due to unmodeled terms including higher order dynamics, parameter mismatches, and unknown disturbances. An active state p_k (extra state) is introduced to describe the equivalent disturbance. Its estimate $\hat{p}_k$ performs the compensation action. p_k is described by (the same equation used in [10] to estimate unknown functions)

$$p_k = \sum_{j=1}^{N} (-1)^{j+1} \frac{N!}{j!(N-j)!} p_{k-j} + {}^{N-1} w_k. \tag{30}$$

The stochastic equation (30) says that the Nth-order derivative (or Nth-order evolution) of p_k is randomly distributed. ${}^{N-1}w_k$ is a Gaussian variable with zero mean. If

$${}^{N-1}w_k = 0 \tag{31}$$

then (30) is a deterministic model for any disturbance p_k that has its Nth derivative equal to zero. In this way, the stochastic information present in ${}^{N-1}w_k$ gives more flexibility to p_k, since its evolutionary model is not rigid.

3) The stochastic design of the Kalman matrices for the AOB context.

Fig. 4 represents the AOB control structure. The first-order AOB algorithm[6] (AOB-1) is summarized in Section IV-A. In this case, p_k is given by (30) with $N = 1$.

[6]The general AOB algorithm uses N extra states to describe $\hat{p}_k$ [6], [9].

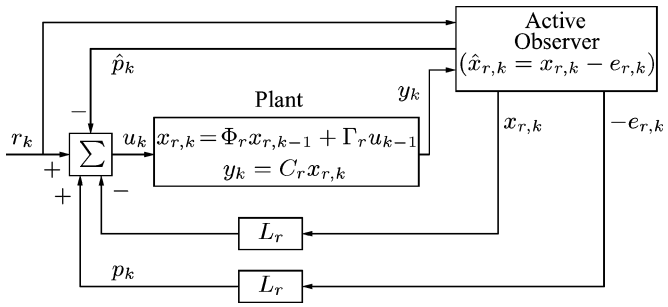

Fig. 4. AOB. The active state $\hat{p}_k$ compensates for the error $e_{r,k}$ referred to the system input. L_r is the state feedback gain.

A. AOB-1 Algorithm

Controlling (18) through state feedback from an observer and inserting p_k and $\hat{p}_k$ in the loop, the overall system can be represented by (see Fig. 4)

$$\begin{bmatrix} x_{r,k} \\ p_k \end{bmatrix} = \begin{bmatrix} \Phi_r & \Gamma_r \\ 0 & 1 \end{bmatrix} \begin{bmatrix} x_{r,k-1} \\ p_{k-1} \end{bmatrix} + \begin{bmatrix} \Gamma_r \\ 0 \end{bmatrix} u_{k-1} + \xi_k \tag{32}$$

$$y_k = C_a [x_{r,k-1} \quad p_{k-1}]^T + \eta_k \tag{33}$$

where

$$u_{k-1} = r_{k-1} - [L_r \quad 1] \begin{bmatrix} x_{r,k-1} \\ \hat{p}_{k-1} \end{bmatrix} \tag{34}$$

$$C_a = [C_r \quad 0]. \tag{35}$$

The stochastic inputs $\xi_k = [\xi_{x_{r,k}} \; {}^0 w_k]^T$ and η_k represent, respectively, model and measure uncertainties. The state estimate of (32) is based on the desired closed loop (i.e., $\hat{p}_k = p_k$ and $\hat{x}_{r,k} = x_{r,k}$). It is

$$\begin{bmatrix} \hat{x}_{r,k} \\ \hat{p}_k \end{bmatrix} = \begin{bmatrix} \Phi_r - \Gamma_r L_r & 0 \\ 0 & 1 \end{bmatrix} \begin{bmatrix} \hat{x}_{r,k-1} \\ \hat{p}_{k-1} \end{bmatrix} + \begin{bmatrix} \Gamma_r \\ 0 \end{bmatrix} r_{k-1} + K_k (y_k - \hat{y}_k) \tag{36}$$

with

$$\hat{y}_k = C_a \left(\begin{bmatrix} \Phi_r - \Gamma_r L_r & 0 \\ 0 & 1 \end{bmatrix} \begin{bmatrix} \hat{x}_{r,k-1} \\ \hat{p}_{k-1} \end{bmatrix} + \begin{bmatrix} \Gamma_r \\ 0 \end{bmatrix} r_{k-1} \right). \tag{37}$$

The Kalman gain K_k reflects the uncertainty associated with each state, which is a function of ξ_k and η_k [3], [22], and is computed as follows:

$$K_k = P_{1k} C_a^T [C_a \, P_{1k} \, C_a^T + R_k]^{-1} \tag{38}$$

with

$$P_{1k} = \Phi_n P_{k-1} \Phi_n^T + Q_k \tag{39}$$

$$P_k = P_{1k} - K_k C_a P_{1k} \tag{40}$$

where Φ_n is the augmented open-loop matrix

$$\Phi_n = \begin{bmatrix} \Phi_r & \Gamma_r \\ 0 & 1 \end{bmatrix}. \tag{41}$$

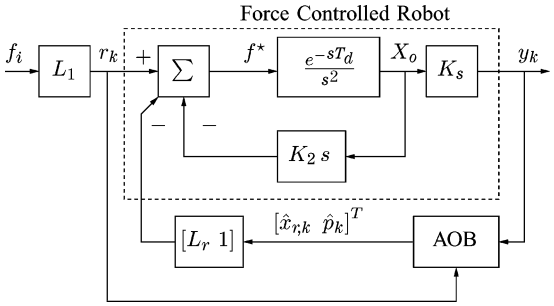

Fig. 5. Compliant motion control with the AOB in the loop. L_1 is the first element of the state feedback gain $L = [L_r\ 1]$, f_i is the force input, and y_k is the force output (measured by the force sensor).

The system noise matrix $Q_k = E\{\xi_k \xi_k^T\}$ can be represented by

$$Q_k = \begin{bmatrix} Q_{x_{r,k}} & 0 \\ 0 & Q_{p_k} \end{bmatrix}. \tag{42}$$

The measurement noise matrix $R_k = E\{\eta_k \eta_k^T\}$. P_k is the mean-square error matrix. Its initial value should reflect the uncertainty in the state estimation. It should not be lower than the initial matrix Q_k. Fig. 5 shows the control architecture with the AOB in the loop.

B. AOB Estimation Strategies for Haptic Manipulation

Model reference adaptive control appears if $Q_{x_{r,k}}$ is much smaller than Q_{p_k}. In this case, the estimation for the system state follows the reference model. Everything that does not fit in the $x_{r,k}$ model goes to p_k. However, for compliant motion tasks (with or without haptic devices), the estimation of force (first state) from the model is very inaccurate, since K_s may have abrupt and unpredictable changes. Providing methods for online stiffness estimation and increasing $Q_{x_{r,k}}$ for the first state creates better conditions to estimate the force. Knowing the structure of Q_k, the relation between R_k and Q_k makes the estimates more (R_k low) or less (R_k high) sensitive to measures, which is reflected in K_k. The state-estimation dynamics increase with K_k [see (36)], as they are limited by robustness and noise-sensitivity requirements. Q_k and R_k are a powerful tool in the control design, creating enough space to explore complex estimation strategies for highly unstructured tasks. In the experiments, the following AOB stochastic matrices for each Cartesian dimension have been used:

$$Q_k = \begin{bmatrix} 10^{-3} & \cdots & 0 & 0 \\ 0 & 10^{-12} & 0 & 0 \\ \vdots & \ddots & \vdots & \vdots \\ 0 & \cdots & 10^{-12} & 0 \\ 0 & \cdots & 0 & 10^{-5} \end{bmatrix} \tag{43}$$

where $R_k = 8.5$ and $P_0 = Q_0$. This design entails the steady-state Kalman gains

$$K_k \times 10^3 \approx [10.9 \quad 1.1 \quad 0.9 \quad 0.9 \quad 0.9 \quad 0.9]^T. \tag{44}$$

The K_k for the first state in (44) is high, due to its relatively high uncertainty in (43). The absolute values of Q_k and R_k are not important, since the same scaling factor applied to both of them entails the same K_k [9]. Therefore, the state estimates in (36) are not affected. It should be pointed out that K_k is not too sensitive to Q_k and R_k, since small changes in the stochastic structure give similar results.

C. Pole Placement for Haptic Manipulation

In force-based tasks, force overshoots/undershoots are usually undesired. Hence, the state feedback gain L_r can be computed by Ackermann's formula to achieve a critically damped system ($\zeta = 1$). The other poles due to T_d should be mapped far away from the dominant poles to neglect their influence in the system response. In our setup, they were mapped at $z = 0$. The closed-loop time constant τ_c should be small enough to enable the task execution with comfortable performance. However, it should not be too small to avoid saturation effects in the command effort. In our setup, we have

$$\tau_c = 3\tau_o \quad \text{and} \quad \tau_o = 25\ \text{ms}. \tag{45}$$

Therefore, the settling time is about $5 \times \tau_c$ (0.375 s), which is adequate for many human-controlled tasks.

D. Free-Space Behavior

The AOB control architecture is kept even for free-space conditions (no control switching). In this case, the force output is always zero ($y_k = 0$). Rewriting (36) as

$$\hat{x}_{e,k} = \Phi_{e,c}\hat{x}_{e,k-1} + \Gamma_e r_{k-1} + K_k(y_k - \hat{y}_k) \tag{46}$$

in free space, (46) becomes

$$\hat{x}_{e,k} = \Phi^f_{e,c}\hat{x}_{e,k-1} + \Gamma^f_e r_{k-1} \tag{47}$$

with

$$\Phi^f_{e,c} = (I - K_k C_a)\Phi_{e,c} \tag{48}$$

$$\Gamma^f_e = (I - K_k C_a)\Gamma_e. \tag{49}$$

The free-space plant is depicted in Fig. 6. The AOB generates a virtual state $\hat{x}_{e,k}$ that enters the system. This plant is not stable. $H^f_1(z)$ has one discrete pole at $z = 1$ due to the active state equation, and $G^f(s)$ has another pole at $s = 0$. Writing the pulse-transfer function[7] of $G^f(s)$ as

$$G^f(z) = \frac{1}{K_2}\frac{b_1 z + b_2}{z^2 + a_1 z + a_2} z^{-T_d/T_s} \tag{50}$$

with

$$\begin{aligned} b_1 &= (K_2 T_s - 1 + e^{-K_2 T_s})/K_2 \\ b_2 &= (1 - e^{-K_2 T_s} - K_2 T_s e^{-K_2 T_s})/K_2 \\ a_1 &= -1 + e^{-K_2 T s} \\ a_2 &= e^{-K_2 T_s} \end{aligned} \tag{51}$$

[7]It is assumed that a zeroth-order hold transforms a discrete signal into a continuous one. A table of the most common pulse-transfer functions can be seen in [1].

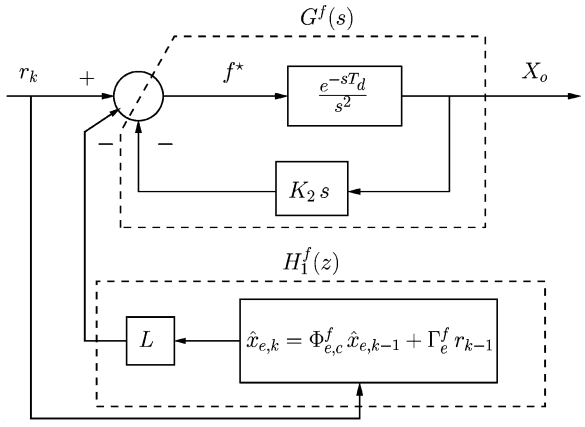

Fig. 6. Free-space plant. The AOB controller generates a virtual state that enters the system. This plant has one continuous pole at $s = 0$ and a discrete pole at $z = 1$.

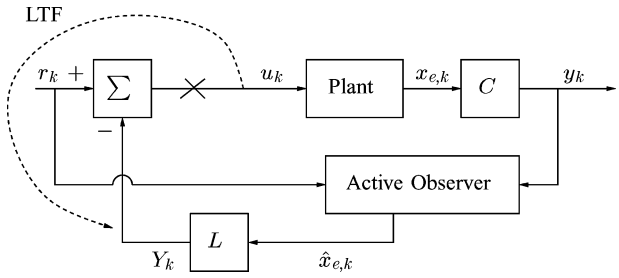

Fig. 7. LTF computation with the AOB in the loop.

then the equivalent transfer function of the free-space plant $G^f_{se}(z)$, also including the preamplification of r_k by L_1, is

$$G^f_{se}(z) = L_1\left[G^f(z) - H^f_1(z)G^f(z)\right] \tag{52}$$

$$H^f_1(z) = L\left(zI - \Phi^f_{e,c}\right)^{-1}\Gamma^f_e. \tag{53}$$

Stability of the whole system is achieved through the teleoperation architecture described in Section VI.

V. AOB Stability and Robustness

Here, we analyze relative stability of AOB-based controllers in the presence of model errors. The loop transfer function[8] (LTF) of the control system has to be derived. A schematic representation of it is depicted in Fig. 7. Applying u_k to the plant input and considering all other inputs zero (necessary to compute the LTF), (32) and (33) can be written as

$$x_{e,k} = \Phi x_{e,k-1} + \Gamma u_{k-1} \tag{54}$$

$$y_k = C x_{e,k} \tag{55}$$

with

$$x_{e,k} = [x_{r,k} \quad p_k]^T. \tag{56}$$

[8]The LTF is the product of the transfer functions of forward and feedback loops. Special attention should be paid when observers are in the loop [15].

The real system matrix Φ is equal to the nominal matrix Φ_n (i.e., the one used in the design) plus the unknown error $\Delta\Phi$ due to unmodeled terms. Mathematically, we have

$$\Phi = \Phi_n + \Delta\Phi. \tag{57}$$

The AOB state estimate is[9] of the form

$$\hat{x}_{e,k} = \Phi_c\hat{x}_{e,k-1} + K_k\left[y_k - C(\Phi_c\hat{x}_{e,k-1})\right] \tag{58}$$

with $\Phi_c = \Phi_n - \Gamma L, \Gamma = [\Gamma_r \quad 0]^T$, and $L = [L_r \quad 1]$. Defining the estimation error e_k as

$$e_k = x_{e,k} - \hat{x}_{e,k} \tag{59}$$

then $\hat{x}_{e,k}$ and e_k can be written as

$$\begin{bmatrix}\hat{x}_{e,k}\\ e_k\end{bmatrix} = \begin{bmatrix}M_{1,1} & K_kC\Phi\\ M_{2,1} & (I - K_kC)\Phi\end{bmatrix}\begin{bmatrix}\hat{x}_{e,k-1}\\ e_{k-1}\end{bmatrix} + \begin{bmatrix}K_kC\Gamma\\ (I - K_kC)\Gamma\end{bmatrix}u_{k-1} \tag{60}$$

where

$$M_{1,1} = \Phi_n - \Gamma L + K_kC(\Delta\Phi + \Gamma L) \tag{61}$$

$$M_{2,1} = (I - K_kC)(\Delta\Phi + \Gamma L). \tag{62}$$

The LTF output is

$$Y_k = [L \quad 0]\begin{bmatrix}\hat{x}_{e,k}\\ e_k\end{bmatrix}. \tag{63}$$

The transfer function of the state-space equations (60) and (63) is the LTF, $H_{\mathrm{LTF}}(z)$, which is given by

$$H_{\mathrm{LTF}}(z) = [L \quad 0][I - \phi z^{-1}]^{-1}\gamma z^{-1} \tag{64}$$

where ϕ and γ are the state transition and command matrices of (60), respectively, and I is the identity matrix. Knowing $H_{\mathrm{LTF}}(z)$, it is straightforward to compute Nyquist/Bode plots and the corresponding phase and gain margins.[10] At very low frequencies, noise statistics make no sense (everything is "static"). The LTF introduces one additional integrator as the AOB order increases, corresponding to the active state equation (30) when ${}^{N-1}w_k \to 0$. Therefore, the system type increases with the AOB order, improving tracking capabilities, although the relative stability decreases.

A. Robustness

In compliant motion tasks, it is important to analyze relative stability when there are stiffness mismatches. From (19), (20), and (1), $d = 3$ and $\tau' = h$. Hence, from (26), $\Gamma_0 = [0 \quad 0]^T$. Moreover, Φ_1 given by (25) does not depend on K_s. If there is a ΔK_s mismatch, $\Delta\Gamma_1$ is given by [see (27)]

$$\Delta\Gamma_1 = \frac{\Delta K_s}{K_{s,n}}\Gamma_1. \tag{65}$$

[9]See (36) for $r_k = 0$.

[10]In the Matlab environment, the LTF representation in state space or transfer function is all that is needed to have Nyquist/Bode plots.

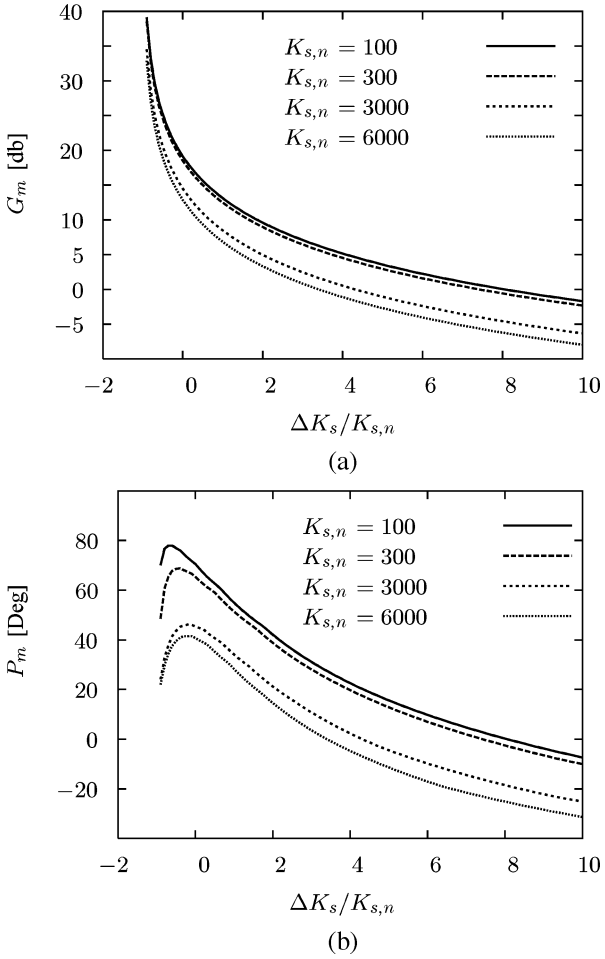

Fig. 8. Robustness to stiffness errors. (a) Gain margin. (b) Phase margin. Stability problems only arise from underestimated stiffness. The values of $K_{s,n}$ are in N/m. Simulation results.

From (22), we have

$$\Delta\Phi_r = \begin{bmatrix} 0 & \Delta\Gamma_1 & 0 & \cdots & 0 \\ 0 & 0 & 0 & \cdots & 0 \\ \vdots & \vdots & \vdots & \ddots & \vdots \\ 0 & 0 & 0 & \cdots & 0 \\ 0 & 0 & 0 & \cdots & 0 \end{bmatrix}. \tag{66}$$

Knowing (41), we have

$$\Delta\Phi = \begin{bmatrix} \Delta\Phi_r & 0 \\ 0 & 0 \end{bmatrix}. \tag{67}$$

Using (60), stability can be analyzed based on the stiffness mismatch. From Fig. 8, it can be inferred that overestimating the stiffness does not create stability problems (negative ΔK_s values). Moreover, robustness increases with $K_{s,n}$. For $K_{s,n} = 100$ N/m, the control structure is stable[11] up to $\Delta K_s \approx 800$ N/m. If $K_{s,n} = 6000$ N/m, the maximum stiffness mismatch is about 400%. This robustness analysis establishes the maximum mismatch between the real stiffness and the nominal one without losing stability, giving an upper bound to the estimation error. Methods for online stiffness estimation are proposed in Section VII.

[11]The full teleoperation scheme discussed in Section VI is not considered in this analysis.

B. Real-Time Issues

This section analyzes properties of AOB-based controllers for online stiffness adaptation. In haptic tasks, contact/noncontact states with stiff objects are critical, since the stiffness changes are big. To achieve consistent force responses independent of the contact object, K_s has to be estimated online to adapt the AOB accordingly.

1) Control Adaptation: The feedback gain L_r of the controller can be easily adapted for new environment stiffnesses without a complete computation of Ackermann's formula. It can be shown [9] that for $K_{s,n}$ with corresponding feedback gains

$$L_r = [l_1 \quad l_2 \quad l_3 \quad \cdots \quad l_n] \tag{68}$$

if $K_{s,n}$ changes ΔK_s, then the new L_r vector should be computed from

$$L_r = [l_1/(1+\Delta K_s/K_{s,n}) \;\; l_2/(1+\Delta K_s/K_{s,n}) \;\; l_3 \;\; \cdots \;\; l_n]. \tag{69}$$

The feedback gains of the state variables due to T_d do not change. Only a proportional factor needs to be computed to update L_r for the "core state."

2) State Estimation: When $K_{s,n}$ changes ΔK_s, the Φ_r matrix changes to $\Phi_r + \Delta\Phi_r$. Only two elements of this matrix have to be recomputed. The Kalman gains K_k are obtained online from (38)–(40). The state estimate of the AOB in (36) needs to be updated, reflecting the changes in Φ_r, L_r, and K_k.

C. Free-Space to Stiff Contact Experiments

This section illustrates the AOB controller without stiffness adaptation. The robot moves from free-space to stiff contact with a desk in the z direction, keeping always $K_{s,n} = 6000$ N/m. When the reference force changes from 0 to 5 N, the robot starts to accelerate due to the active state, till it reaches the desk, where nearly 100 N are measured [see Fig. 9(a) and (c)]. Taking a closer look at the impact data [see Fig. 9(c)], the measured force is always negative, which means that the transition from free space to stiff contact has no bouncing effects. While in contact, the force response follows a critically damped response [see Fig. 9(a) and (d)], with a time constant that is bigger than expected [see (45)]. This means that the value for $K_{s,n}$ is bigger than K_s. The active state reflects this mismatch, increasing its value during the step input, helping the robot to push more in the z-direction, as shown in Fig. 9(c), around 74 s. The position data cannot be used in a consistent way. When the measured force changes smoothly from -5 to -10 N, the measured position does not change in the same way [see Fig. 9(d)], creating problems for online stiffness estimation. The force response drops about 3 N (around 74 s), keeping the same position data. Additionally, a slight change in the force makes a relatively big change in the position. These effects make position measurements not recommended for online stiffness inference, motivating the exploration of adaptive control techniques only based on force data.

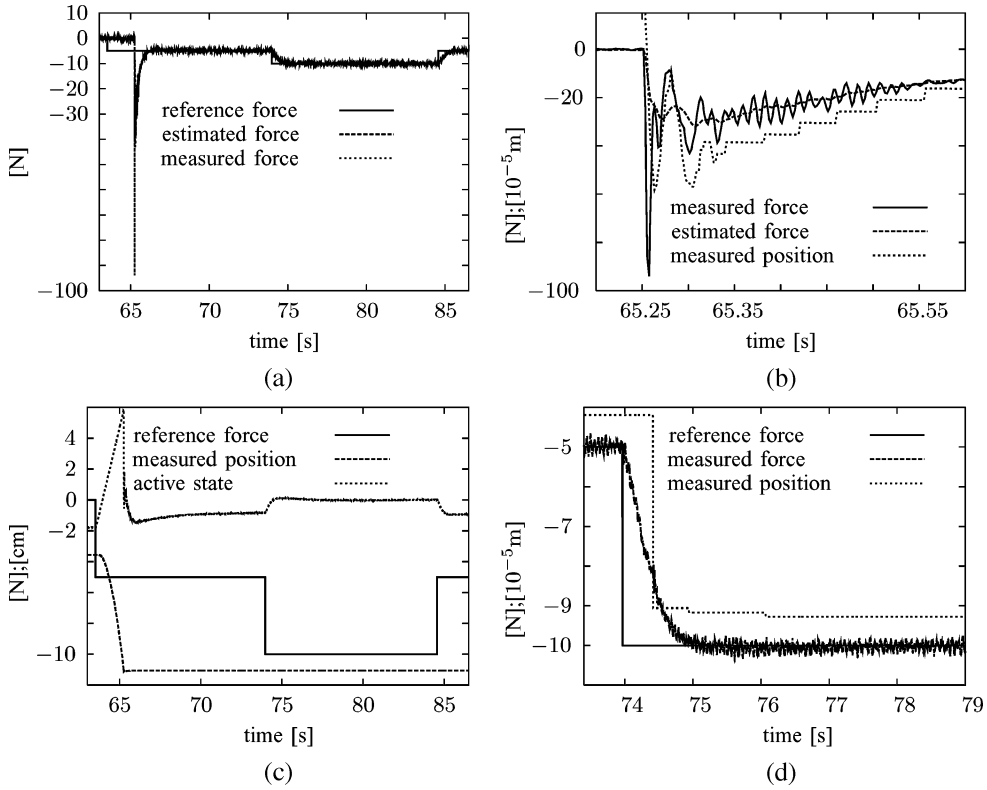

Fig. 9. Experimental results of the AOB controller. Free-space to stiff contact (desk) in the z direction. (a) Force response. (b) Zoom of the impact data. (c) Active state and position data. (d) Zoom of force and position responses. The position data in (b)–(d) were rescaled and shifted by a constant value to match the vertical scale.

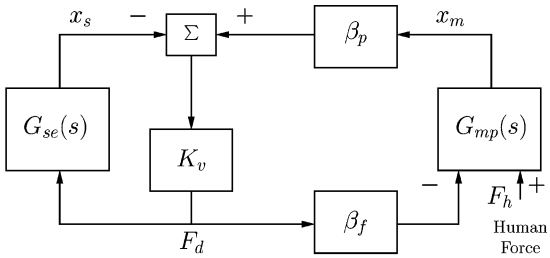

Fig. 10. Teleoperation scheme. $G_{se}(s)$ represents the PUMA robot, the AOB and the environment, and $G_{mp}(s)$ represents the master station, including the human arm and the haptic device.

VI. Teleoperation Scheme

Fig. 10 illustrates the teleoperation scheme for each direction in operational space. x_m, x_s, β_p, and β_f are the master position, slave position, position scaling, and force scaling, respectively. $G_{se}(s)$ represents the slave station, including the robotic manipulator, the AOB, and the environment. $G_{se}(s)$ can be split into two functions, describing contact and free-space conditions. $G_{mp}(s)$ is the master station, which includes the haptic device and the human arm. It can be represented by [36]

$$G_{mp}(s) = \frac{1}{m_m s^2 + c_m s + K_m} \tag{70}$$

where m_m, c_m, and K_m are, respectively, the mass, damping, and stiffness of the master station.[12] This teleoperation scheme is similar to a position–position architecture with some differences.

[12] K_m is mainly due to the human arm stiffness.

The input to the master and slave is the desired force F_d, generated by position errors through the virtual coupling K_v. The AOB commands the slave device to track F_d with a desired dynamics. There is no force controller at the master station, which receives F_d scaled by β_f. In the teleoperation experiments

$$\begin{aligned} K_v &= 1000 \text{ N/m} \\ \beta_p &= 2.0 \\ \beta_f &= 0.1. \end{aligned} \tag{71}$$

A. Teleoperation in Contact

For the control design proposed in this paper, the desired transfer function $G_{se}(s)$ while in contact is

$$G_{se}(s) = \frac{1}{K_{s,n}} \frac{(1/\tau_c)^2}{(s+1/\tau_c)^2} e^{-sT_d} \approx \frac{1}{K_{s,n}} \frac{(1/\tau_c)^2}{(s+1/\tau_c)^2} \tag{72}$$

which means that the force response is critically damped with time constant τ_c, as discussed in Section IV-C.

1) Telepresence: The quality of the haptic feeling is analyzed by investigating the transfer function[13] from the human force to the master position [26]. Looking to Fig. 11, telepresence is achieved if $X_m(s)/F_h(s)$ is of form

$$\frac{X_m(s)}{F_h(s)} = \frac{1}{m_m s^2 + c_m s + (\alpha_s K_s + K_m)} \tag{73}$$

[13] The Laplace transforms of x_m and f_h are $X_m(s)$ and $F_h(s)$, respectively.

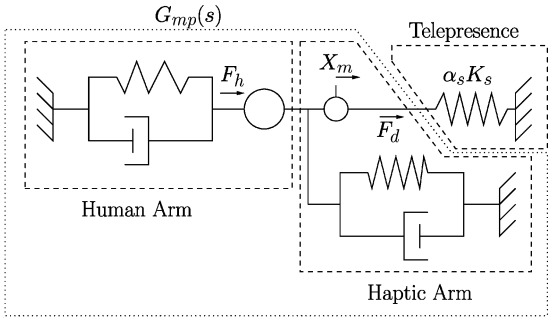

Fig. 11. Teleoperation with telepresence. Both human and haptic arms are represented by spring–damper–mass systems.

where α_s is a positive constant.[14] From Fig. 10, we have

$$\frac{X_m(s)}{F_h(s)} = \frac{1/(m_m s^2 + c_m s + K_m)}{1 + \frac{K_v \beta_p \beta_f}{(1+G_{se}(s)K_v)(m_m s^2 + c_m s + K_m)}}. \quad (74)$$

For the general case, the effect of the slave term $G_{se}(s)$ in (74) depends on human arm parameters that vary during the task execution, which is hard to quantify.

At low frequencies, (74) is approximated by

$$\frac{X_m(s)}{F_h(s)}_{s\to 0} = \frac{1}{K_m\left(1 + \frac{K_v \beta_p \beta_f}{(1+K_v/K_{s,n})K_m}\right)}. \quad (75)$$

If $K_v \gg K_{s,n}$, then (75) becomes

$$\frac{X_m(s)}{F_h(s)}_{s\to 0} \approx \frac{1}{K_m + K_{s,n}\beta_p \beta_f}. \quad (76)$$

Comparing (76) with (73) when $s \to 0$, it can be inferred that there is telepresence if $K_{s,n} \propto K_s$. Therefore, enhanced telepresence can be achieved increasing K_v while in contact, making

$$K_v \propto K_s. \quad (77)$$

If $K_v \ll K_{s,n}$, then (75) becomes

$$\frac{X_m(s)}{F_h(s)}_{s\to 0} \approx \frac{1}{K_m + K_v \beta_p \beta_f}. \quad (78)$$

In this case, there is no telepresence. The user only feels K_v.

At high frequencies, (74) is approximated by

$$\frac{X_m(s)}{F_h(s)} \approx \frac{1}{m_m s^2 + c_m s + K_m} \quad (79)$$

which means that only the master station is felt.

2) Stability: Let us consider $G_{se}(s)$ of the form[15]

$$G_{se}(s) = \frac{K_f}{(s+p_1)(s+p_2)} \quad (80)$$

[14]For nanomanipulation schemes, augmented reality may require $\alpha_s > 1$. On the other hand, scaling down the real stiffness ($\alpha_s < 1$) may help to distinguish differences between stiff objects.

[15]See the desired closed-loop plant in (72).

where $p_1 > 0$, $p_2 > 0$, and $K_f > 0$. From (74) and (80), the characteristic polynomial $P_\Delta(s)$ is given by

$$P_\Delta(s) = A_\Delta s^4 + B_\Delta s^3 + C_\Delta s^2 + D_\Delta s + E_\Delta \quad (81)$$

where

$$\begin{aligned} A_\Delta &= m_m \\ B_\Delta &= c_m + (p_1+p_2)m_m \\ C_\Delta &= K_v\beta_f\beta_p + (p_1+p_2)c_m + K_m + (K_f K_v + p_1 p_2)m_m \\ D_\Delta &= (K_f K_v + p_1 p_2)c_m + (p_1+p_2)(K_m + K_v\beta_f\beta_p) \\ E_\Delta &= (K_f K_v + p_1 p_2)K_m + K_v p_1 p_2 \beta_f \beta_p. \end{aligned} \quad (82)$$

From (82), $A_\Delta > 0$ and $B_\Delta > 0$. Hence, applying the Routh–Hurwitz stability criterion, the system is stable if

$$C_\Delta - D_\Delta A_\Delta / B_\Delta > 0 \quad (83)$$

$$D_\Delta - E_\Delta B_\Delta^2 / (B_\Delta C_\Delta - D_\Delta A_\Delta) > 0. \quad (84)$$

Algebraic manipulation shows that (83) only has positive terms, but (84) has a negative term.[16] To eliminate the influence of this negative term, a sufficient condition for stability [i.e., it guarantees (84)] is

$$K_m < \frac{K_v(p_1+p_2)\beta_p\beta_f m_m}{2c_m}. \quad (85)$$

B. Teleoperation in Free-Space

The unstable free-space plant described in (52) is stabilized by the teleoperation system through position feedback.

1) Telepresence: In discrete terms, applying the z-transform

$$\frac{X_m(z)}{F_h(z)} = \frac{G_{mp}(z)}{1 + \beta_p\beta_f K_v G_{mp}(z) \Big/ \left(1 + G_{se}^f(z)K_v\right)} \quad (86)$$

where $G_{mp}(z)$ is the pulse-transfer function of $G_{mp}(s)$. For the general case, the effect of the slave term $G_{se}^f(z)$ in (86) depends on human arm parameters, which are not known in advance.

At low frequencies, we have

$$G_{se}^f(z)_{z\to 1} \to \infty \quad (87)$$

due to the poles at $z = 1$ and $s = 0$ (see Section IV-D). Therefore, (86) becomes

$$\frac{X_m(z)}{F_h(z)} \approx G_{mp}(z) \to \frac{1}{K_m}. \quad (88)$$

Equation (88) shows telepresence in free-space, since only the master station is felt.

At high frequencies, all transfer functions converge to zero. Hence, (86) is given by

$$\frac{X_m(z)}{F_h(z)} \approx G_{mp}(z) \to 0. \quad (89)$$

[16]This analysis can be checked through the Mathematica command $\mathrm{FullSimplify}[\mathrm{Factor}[D_\Delta - E_\Delta B_\Delta^2/(B_\Delta C_\Delta - D_\Delta A_\Delta)]]$.

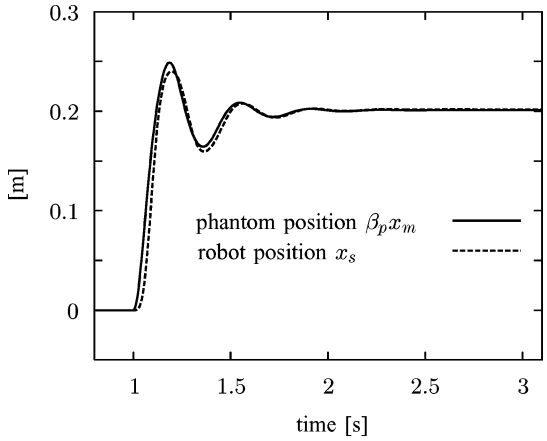

Fig. 12. Haptic manipulation in free-space. Position response after applying a force input F_h of 10 N at 1 s. K_m is equal to $K_{s,n}$. Simulation results.

Equation (89) shows again that only the master station is felt (there is telepresence).

2) Stability: The position-tracking capabilities can be inferred from (see Fig. 10)

$$\frac{X_s(z)}{X_m(z)} = \frac{\beta_p K_v G_{se}^f(z)}{1 + K_v G_{se}^f(z)} \tag{90}$$

where $X_s(z)$ is the z-transform of x_s. K_v should be designed such that (90) has proper closed-loop dynamics and (86) is stable for a wide range of K_m, m_m, and c_m. Making

$$K_v = 1000 \text{ N/m} \tag{91}$$

and considering that for a light phantom manipulation (the usual situation in free-space)

$$K_m = 100 \text{ N/m} \tag{92}$$
$$m_m = 0.30 \text{ kg} \tag{93}$$
$$c_m = m_m/100 \text{ kg/s} \tag{94}$$

then the computation of the closed-loop poles in (86) and (90) is straightforward. A step input F_h of 10 N at 1 s originates the position responses represented in Fig. 12, showing that position commands issued by the human arm are well tracked by the robot. This control setup guarantees stability for a wide range of K_m, m_m, and c_m. As K_v increases, the stability margins of (86) decrease, which can be critical if the human arm becomes stiff.

VII. Online Stiffness Estimation

Online stiffness estimation is a key issue to enhancing telepresence in contact tasks. The main novelty of our method, with respect to previous work (see [16] for a comparative study), is that only force data are used to estimate the stiffness. The force estimation can be compared with desired and real forces to update $K_{s,n}$.

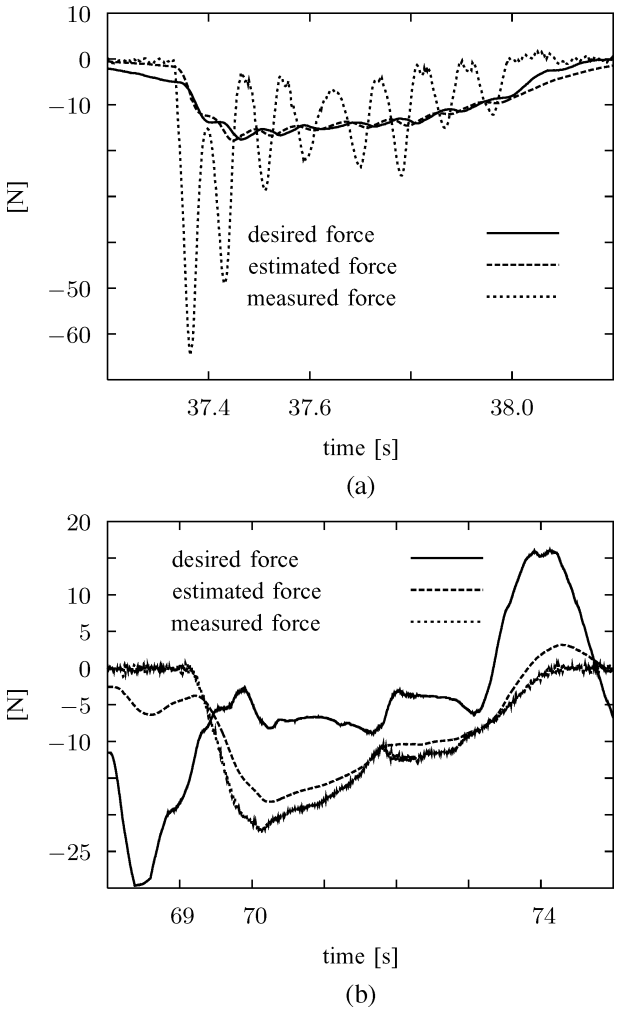

Fig. 13. Teleoperation data without stiffness adaptation. (a) Underestimated stiffness. $K_{s,n} = 100$ N/m and K_s changes from free-space to stiff contact (book). (b) Overestimated stiffness. $K_{s,n} = 3000$ N/m and K_s changes from free-space to soft contact (sponge).

A. Stiffness Adaptation Algorithm

The relation between measured and estimated forces (f_m and f_e, respectively) gives useful information about K_s.

There are two cases.

1) K_s is bigger than $K_{s,n}$.
2) K_s is smaller than $K_{s,n}$.

Fig. 13(a) illustrates the first case. The system may become unstable such that f_m fluctuates around f_e. The difference between the desired force f_d and f_e is relatively small, compared with the difference between f_m and f_e. In the second case, represented in Fig. 13(b), the difference between f_d and f_e is bigger than the difference between f_m and f_e.

Based on these results, the following adaptation law is proposed:

$$K_{s,1}^i = K_{s,1}^{i-1} + \Delta \hat{K}_{s,1}^i \tag{95}$$

where

$$\Delta \hat{K}_{s,1}^i = K_{s,u} + K_{s,o} \tag{96}$$
$$K_{s,u} = k_1 |f_m - f_e| \sigma_d \left(c, \frac{|f_m - f_e|}{|f_e| + a_1} - b_1 \right) \tag{97}$$

TABLE II
NUMERICAL VALUES OF THE DESIGN PARAMETERS FOR STIFFNESS ADAPTATION

a_1	1.0	f_0	20.0	[N]
a_2	0.1	k_1	10.0	[m^{-1}]
b_1	1.5	k_2	10.0	[m^{-1}]
b_2	1.0	k_3	3000.0	[N/m]
c	5.0	l_1	0.05	
c_0	0.2	l_2	0.02	

$$K_{s,o} = -k_2|f_d - f_e|\sigma_d\left(c, \frac{|f_d - f_e|}{|f_e| + a_2} - b_2\right) \quad (98)$$

$$\sigma_d(c,x) = \frac{1}{1 + e^{-cx}} \quad (99)$$

where $k_1, k_2, a_1, a_2, b_1, b_2$, and c are positive parameters. The upper script i denotes the discrete time step. $K_{s,u}$ in (97) corrects errors due to underestimated stiffness, and $K_{s,o}$ in (98) is for overestimated stiffness. The general sigmoid function $\sigma_d(c, x_1 - x_2)$ acts as a smooth switch of x_1 centered around x_2. The parameter c defines the smoothing factor. a_1 and a_2 avoid ill-conditioned results when f_e is close to zero. The minimum value of $\hat{K}_{s,1}$ is set to zero. Offline analysis has shown that the object stiffness increases with applied force. Equation (100) adjusts the stiffness for this problem

$$\hat{K}_{s,2} = K_{\min} + k_3\sigma_d\left(c_0, |f_m - f_0|\right) \quad (100)$$

where f_0, c_0, and k_3 are positive parameters. f_0 indicates the force from which $\hat{K}_{s,2}$ is increased, and $K_{\min}$ is the minimum stiffness of $\hat{K}_{s,2}$.

Finally, low-pass filters are used to prevent jerky motions due to quick changes in the stiffness estimation. The filter should not introduce too much time lag, otherwise, the user may feel a "sticky" behavior when the contact is released. The filter equations are

$$\hat{K}^{f,i}_{s,1} = \hat{K}^{f,i-1}_{s,1} + l_1\left(\hat{K}^{i}_{s,1} - \hat{K}^{f,i-1}_{s,1}\right) \quad (101)$$

$$\hat{K}^{f,i}_{s,2} = \hat{K}^{f,i-1}_{s,2} + l_2\left(\hat{K}^{i}_{s,2} - \hat{K}^{f,i-1}_{s,2}\right). \quad (102)$$

The complete estimation algorithm given by

$$K_{s,n} = \hat{K}^{f,i}_{s,1} + \hat{K}^{f,i}_{s,2} \quad (103)$$

is the sum of (101) and (102). The minimum value of $K_{s,n}$ is $K_{\min}$ from (100). In the experiments, $K_{\min} = 100$ N/m. The other parameters are shown in Table II. Note that $\hat{K}_{s,1}$ is a function of f_e, which depends on the estimation strategy. Therefore, Table II is correlated with the AOB design.

VIII. HAPTIC MANIPULATION EXPERIMENTS

Fig. 14 shows teleoperation experiments using the AOB with online stiffness adaptation. Three contact surfaces were tested (sponge, book, and table) with free-space transitions. The stiffness that the user perceives depends on human arm parameters [see (74) and (86)], which cannot be directly inferred from

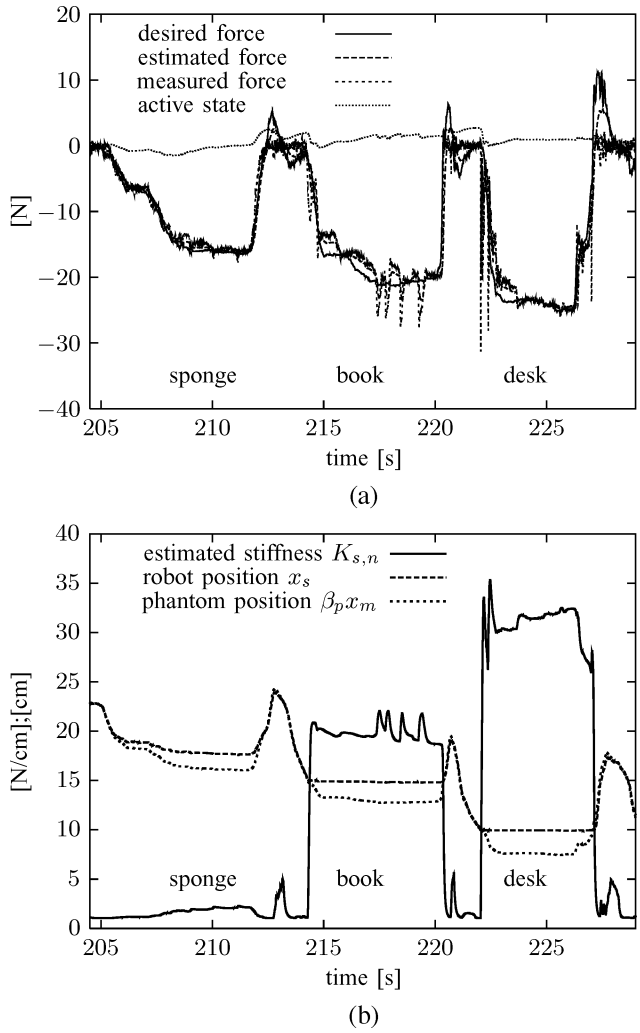

Fig. 14. Teleoperation data with the AOB and adaptation in the z direction. Sponge, book and desk contacts. (a) Force and active state data. (b) Robot position x_s versus phantom position $\beta_p x_m$. Online stiffness estimation.

Fig. 14. For the sponge contact, telepresence is achieved [see (76)]. The book and desk are stiffer than K_v, decreasing telepresence. In the experiments, the virtual coupling and scaling factors given by (71) limit the haptic feeling quality of stiff objects [see (78)]. This problem can be solved by (77). K_v adaptation techniques are not addressed in this study.

Fig. 14(a) shows the control performance. Measured and estimated forces closely match the desired one independent of the contact surface. The active state is more "active" during free-space-to-contact (and vice versa) transitions, due to bigger modeling errors. Moving up the phantom in free-space (contact-to-free-space transitions), a positive force F_d is created, since the phantom position goes ahead of the robot position. On the other hand, if the phantom is moving down, F_d becomes negative. This drag effect is felt by the user in free-space motion, being calibrated by K_v [see (90)].

The stiffness estimation reflects the real stiffness, distinguishing the sponge, book, and desk at the beginning of contact [see Fig. 14(b)].

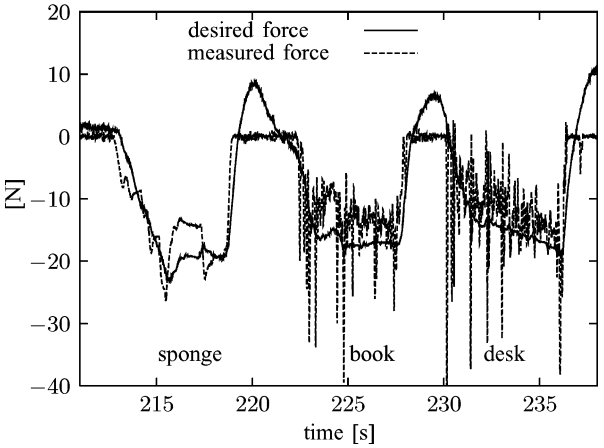

Fig. 15. Teleoperation data with a PID controller in the z-direction. Sponge, book, and desk contacts. Force data.

Big position-tracking errors indicate contact. These errors generate forces through K_v that are felt at the master station. For instance, at 225 s, we have

$$\beta_p x_m - x_s \approx -2.5\,\text{cm} \tag{104}$$

which entails (Fig. 10)

$$F_d = K_v(\beta_p x_m - x_s) \approx -25\,\text{N}. \tag{105}$$

This means that the phantom arm (i.e., x_m) moved down about 1.25 cm from the beginning of desk contact.

The same experiment with a proportional-integral-derivative (PID)-based controller on the slave side is presented in Fig. 15. The PID gains were experimentally tuned to improve the overall performance. The derivative gain $D_g = 0$ to avoid force sensor noise amplification. The integral and proportional gains were, respectively, set to $I_g = 0.1$ and $P_g = 0.05$. This design was chosen to guarantee stability on hard contact, affecting the performance in free-space due to small bandwidth. This effect can be seen by high F_d around 220, 229, and 237 s. Good results were achieved in sponge contact, but stiffer contacts were marginally stable.

The AOB control scheme with online stiffness adaptation significantly improved telepresence in contact and free-space with respect to PID-based solutions.

IX. Conclusion

This paper has presented an adaptive compliant motion controller with Kalman AOBs, which run on top of operational space and feedback linearization techniques. This controller has been applied in a teleoperation system with small time delay, consisting of a robotic manipulator connected to a haptic device through virtual coupling. No control switching between contact/noncontact states is required. Stochastic estimation strategies for haptic manipulation have been proposed. If the system model is inaccurate, sensor-based estimations should be followed. Stability and robustness analysis have shown that online stiffness adaptation is necessary if the robot manipulates soft and stiff objects. Real-time methods have been presented to adapt the state estimation and the control gains when there are stiffness changes. Only force signals have been used to estimate the stiffness (measured, desired, and estimated forces). Sigmoid functions, online filtering, and offline analysis are important to tune stiffness estimation parameters. Stability and telepresence of the teleoperation scheme have been discussed. The virtual coupling established the tradeoff between telepresence in contact and robustness and comfortable performance in free space. Experiments have shown good results in contact with soft and stiff surfaces, improving telepresence with respect to PID-based solutions.

References

[1] K. J. Åström and B. Wittenmark, *Computer Controlled Systems: Theory and Design*. Englewood Cliffs, NJ: Prentice-Hall, 1997.
[2] N. Bajcinca, R. Cortesão, and M. Hauschild, "Robust control for steer-by-wire vehicles," *Auton. Robots*, vol. 19, pp. 193–214, 2005.
[3] S. M. Bozic, *Digital and Kalman Filtering*. London, U.K.: E. Arnold, 1979.
[4] P. Coelho and U. Nunes, "Path-following control of mobile robots in presence of uncertainties," *IEEE Trans. Robot.*, vol. 21, no. 2, pp. 252–261, Apr. 2005.
[5] J. Colgate and N. Hogan, "Robust control of dynamically interacting systems," *Int. J. Control*, vol. 48, no. 1, pp. 65–88, 1988.
[6] R. Cortesão, "Kalman techniques for intelligent control systems: Theory and robotic experiments," Ph.D. dissertation, Elect. Comput. Eng. Dept., Univ. of Coimbra, Coimbra, Portugal, 2003.
[7] R. Cortesão and N. Bajcinca, "Model-matching control for steer-by-wire vehicles with under-actuated structure," in *Proc. Int. Conf. Intell. Robots Syst.*, 2004, pp. 1148–1153.
[8] R. Cortesão, R. Koeppe, U. Nunes, and G. Hirzinger, "Force control with a Kalman active observer applied in a robotic skill transfer system," *Int. J. Mach. Intell. Robot. Control, Special Issue on Force Control Adv. Robot. Syst.*, vol. 2, no. 2, pp. 59–68, Jun. 2000.
[9] ——, "Compliant motion control with stochastic active observers," in *Proc. Int. Conf. Intell. Robots Syst.*, 2001, pp. 1876–1881.
[10] ——, "Data fusion for robotic assembly tasks based on human skills," *IEEE Trans. Robot.*, vol. 20, no. 6, pp. 941–952, Dec. 2004.
[11] R. Cortesão, J. Park, and O. Khatib, "Real-time adaptive control for haptic manipulation with active observers," in *Proc. Int. Conf. Intell. Robots Syst.*, 2003, pp. 2938–2943.
[12] ——, "Telepresence and stability analysis for haptic telemanipulation with short time delay," in *Proc. Int. Conf. Intell. Robots Syst.*, 2005, pp. 3146–3151.
[13] R. Daniel and P. McAree, "Fundamental limits of performance for force reflecting teleoperation," *Int. J. Robot. Res.*, vol. 17, no. 8, pp. 811–830, Aug. 1998.
[14] P. Dario, B. Hannaford, and A. Menciassi, "Smart surgical tools and augmenting devices," *IEEE Trans. Robot. Autom.*, vol. 19, no. 5, pp. 782–792, Oct. 2003.
[15] J. Doyle and G. Stein, "Robustness with observers," *IEEE Trans. Autom. Control*, vol. AC-24, no. 4, pp. 607–611, Aug. 1979.
[16] D. Erickson, M. Weber, and I. Sharf, "Contact stiffness and damping estimation for robotic systems," *Int. J. Robot. Res.*, vol. 22, no. 1, pp. 41–57, 2003.
[17] H. Flemmer, B. Eriksson, and J. Wikander, "Control design for transparent teleoperators with model parameter variation," in *Proc. Int. Conf. Robot. Autom.*, 2002, pp. 2956–2961.
[18] A. Frisoli, F. Rocchi, S. Marcheschi, A. Dettori, F. Salsedo, and M. Bergamasco, "A new force-feedback arm exoskeleton for haptic interaction in virtual environments," in *Proc. World Haptics Conf.*, Pisa, Italy, 2005, pp. 195–201.
[19] B. Hannaford and J. Ryu, "Time-domain passivity control of haptic interfaces," *IEEE Trans. Robot. Autom.*, vol. 18, no. 1, pp. 1–10, Feb. 2002.
[20] K. Hashtrudi-Zaad and S. E. Salcudean, "Transparency in time-delayed systems and the effect of local force feedback for transparent teleoperation," *Int. J. Robot. Autom.*, vol. 18, no. 1, pp. 108–114, Feb. 2002.
[21] M. Hernando, E. Gambao, E. Pinto, and A. Barrientos, "Collision control in teleoperation by virtual force reflection. An application to the robtet system," in *Proc. Int. Conf. Robot. Autom.*, Detroit, MI, 1999, vol. 1, pp. 565–570.

[22] A. Jazwinsky, *Stochastic Processes and Filtering Theory*, R. Bellman, Ed. New York: Academic, 1970, vol. 64, Mathematics in Science and Engineering.
[23] O. Khatib, "A unified approach for motion and force control of robot manipulators: The operational space formulation," *Int. J. Robot. Autom.*, vol. 3, no. 1, pp. 43–53, Feb. 1987.
[24] W. S. Kim, B. Hannaford, and A. K. Bejczy, "Force-reflecting and shared compliant control in operating telemanipulators with time delay," *Int. J. Robot. Autom.*, vol. 8, pp. 176–185, Apr. 1992.
[25] Y. Landau, "A survey of model reference adaptive techniques. Theory and applications," *Int. J. Automatica*, vol. 10, no. 3, pp. 353–379, Jul. 1974.
[26] D. Lawrence, "Stability and transparancy in bilateral teleoperation," *IEEE Trans. Robot. Autom.*, vol. 9, no. 5, pp. 624–637, Oct. 1993.
[27] R. Maia, R. Cortesão, U. Nunes, V. Silva, and F. Fonseca, "Robust low level motion control of a wmr with stochastic active observers," in *Proc. Int. Conf. Adv. Robot.*, 2003, pp. 876–882.
[28] G. Niemeyer and J. Slotine, "Stable adaptive teleoperation," *IEEE J. Oceanic Eng.*, vol. 16, no. 1, pp. 152–162, Jan. 1991.
[29] J. Park, R. Cortesão, and O. Khatib, "Robust and adaptive teleoperation for compliant motion tasks," in *Proc. Int. Conf. Adv. Robot.*, 2003, pp. 513–519.
[30] ——, "Multi-contact compliant motion control for robotic manipulators," in *Proc. IEEE Int. Conf. Robot. Autom.*, 2004, pp. 4789–4794.
[31] J. Park and O. Khatib, "Multi-link multi-contact force control for manipulators," in *Proc. Int. Conf. Robot. Autom.*, 2005, pp. 3624–3629.
[32] A. Peer, B. Stanczyk, and M. Buss, "Haptic telemanipulation with dissimilar kinematics," in *Proc. Int. Conf. Intell. Robots Syst.*, 2005, pp. 2483–2488.
[33] J. Ryu and D. Kwon, "A novel adaptive bilateral control scheme using dual closed-loop dynamic characteristics of master/slave manipulators," in *Proc. Int. Conf. Intell. Robots Syst.*, 2000, pp. 371–376.
[34] J. De Schutter and H. Van Brussel, "Compliant robot motion, I. A formalism for specifying compliant motion tasks. II. A control approach based on external control loops," *Int. J. Robot. Res.*, pp. 3–33, 1988.
[35] R. Taylor and D. Stoianovici, "Medical robotics in computer-integrated surgery," *IEEE Trans. Robot. Autom.*, vol. 19, no. 5, pp. 765–781, Oct. 2003.
[36] Y. Yokokohji and T. Yoshikawa, "Bilateral control of master-slave manipulators for ideal kinesthetic coupling—formulation and experiment," *IEEE Trans. Robot. Autom.*, vol. 10, no. 5, pp. 605–620, Oct. 1994.
[37] M. Zhu and S. E. Salcudean, "Achieving transparency for teleoperator systems under position and rate control," in *Proc. IEEE/RSJ Int. Conf. Intell. Robots Syst.*, Pittsburgh, PA, 1995, vol. 2, pp. 7–12.
[38] W. Zhu and S. Salcudean, "Stability guaranteed teleoperation: An adaptive motion/force control approach," *IEEE Trans. Autom. Control*, vol. 45, no. 11, pp. 1951–1969, Nov. 2000.
[39] R. Cortesão, "On Kalman active observers," in *International Journal on Intelligent and Robotic Systems*. New York: Springer, 2006, to be published.

Rui Cortesão (M'05) received the B.Sc. ("Licenciatura") degree in electrical engineering, the M.Sc. degree in systems and automation, and the Ph.D. degree in control and instrumentation, all from the University of Coimbra, Coimbra, Portugal, in 1994, 1997, and 2003, respectively.

He has been a Visiting Researcher with DLR (1998–2003), Stanford University (2002), and LIRMM-CNRS (2004–2006), where he was involved with compliant motion control, data fusion, steer-by-wire, haptic manipulation, and surgical robotics. He has been a Researcher with the Institute of Systems and Robotics (ISR-Coimbra) since 1994, and an Assistant Professor with the Electrical and Computer Engineering Department, University of Coimbra, where he teaches medical robotics and digital control.

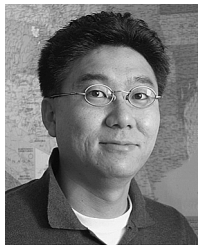

Jaeheung Park (S'98) received the B.S. and M.S. degrees in aerospace engineering from Seoul National University, Seoul, Korea, in 1995 and 1999, respectively. He is currently working toward the Ph.D degree in the Aeronautics and Astronautics Department, Stanford University, Stanford, CA.

He is currently with the Manipulation Group at the Stanford Artificial Intelligence Laboratory. His main research areas are contact force control, robust haptic teleoperation, and whole-body dynamic control of humanoid robots.

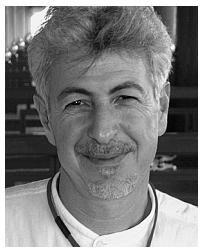

Oussama Khatib (M'85–SM'98–F'03) received the Ph.D. degree from Sup'Aero, Toulouse, France, in 1980.

He is currently a Professor of Computer Science with Stanford University, Stanford, CA. His current research is in human-centered robotics, human motion synthesis, humanoid robotics, dynamic simulation, haptic interfaces, and human-friendly robot design. This builds upon a large body of work pursued over the past 25 years and published in over 200 contributions in the field. He was Program Chair of ICRA2000 and editor of *The Robotics Review*. He served as Director of the Stanford Computer Forum, and is currently President of the International Foundation of Robotics Research and Editor of Springer's *Tracts in Advanced Robotics.*

Prof. Khatib is a Distinguished Lecturer of the IEEE and was a recipient of the JARA Award.